International Journal of Extreme Manufacturing

Will high-entropy carbides and borides be enabling materials for extreme environments?

OPEN ACCESS
IOP Publishing | IMMT
International Journal of Extreme Manufacturing
Int. J. Extrem. Manuf. **5** (2023) 022002 (12pp)
https://doi.org/10.1088/2631-7990/acbd6e

Topical Review

Will high-entropy carbides and borides be enabling materials for extreme environments?

Fei Wang[1], **Frederic Monteverde**[2] **and Bai Cui**[1,3,*]

[1] Department of Mechanical & Materials Engineering, University of Nebraska–Lincoln, Lincoln, NE 68588, United States of America
[2] National Research Council of Italy—Institute of Science, Technology and Sustainability for Ceramics, I-48018 Faenza, Italy
[3] Nebraska Center for Materials and Nanoscience, University of Nebraska–Lincoln, Lincoln, NE 68588, United States of America

E-mail: bcui3@unl.edu

Received 30 May 2022, revised 12 December 2022
Accepted for publication 20 February 2023
Published 9 March 2023

Abstract

The concept of multi-principal component has created promising opportunities for the development of novel high-entropy ceramics for extreme environments encountered in advanced turbine engines, nuclear reactors, and hypersonic vehicles, as it expands the compositional space of ceramic materials with tailored properties within a single-phase solid solution. The unique physical properties of some high-entropy carbides and borides, such as higher hardness, high-temperature strength, lower thermal conductivity, and improved irradiation resistance than the constitute ceramics, have been observed. These promising properties may be attributed to the compositional complexity, atomic-level disorder, lattice distortion, and other fundamental processes related to defect formation and phonon scattering. This manuscript serves as a critical review of the recent progress in high-entropy carbides and borides, focusing on synthesis and evaluations of their performance in extreme high-temperature, irradiation, and gaseous environments.

Keywords: high-entropy ceramics, high-entropy materials, extreme environments, ceramics

1. Introduction

Key structural components in next-generation nuclear reactors, turbine engines, and hypersonic vehicles require novel materials that can fulfill the needs of extreme environments, including high temperatures, chemical reactivities, neutron irradiation, and corrosive coolants. To operate in such harsh environments, materials must possess outstanding physical and chemical properties, such as superior resistance to various external stimuli such as creep, thermal shock, oxidation, or irradiation damage at elevated temperatures. Materials currently in use or under consideration, including stainless steels, nickel superalloys, refractory metals, and SiC, are unsuited to meet one or more property requirements at high temperatures.

The 'multi-principal component' concept has introduced promising opportunities for discovering novel materials.

* Author to whom any correspondence should be addressed.

2631-7990/23/022002+12$33.00

High-entropy alloys (HEAs), a subset of the single-phase concentrated solid-solution alloys [1], have gained significant attention in recent years [2]. Different from traditional alloys, HEAs contain four or more metallic elements in equimolar or near-equimolar concentrations and can form a stable single-phase lattice structure [3], such as FeNiMnCr [4] or $Ti_2ZrHfV_{0.5}Mo_{0.2}$ [5]. The 'multi-principal component' concept has been also used to develop novel thermoelectric materials, such as GeTe-based thermoelectric alloy $Ge_{0.61}Ag_{0.11}Sb_{0.13}Pb_{0.12}Bi_{0.01}Te$ [6] and high-entropy chalcogenide $Pb_{0.89}Sb_{0.012}Sn_{0.1}Se_{0.5}Te_{0.25}S_{0.25}$ [7, 8]. Compared to the widely reported HEAs, high-entropy ceramics (HECs) are more recently discovered and for that reason investigated to a lesser extent. HECs are characterized by at least four metallic elements in an equal or near-equal atomic ratio in the M position (M = metal), while a nonmetal element occupies the X positions (X = C, B, N, or O). HECs include oxides [9, 10], diborides [11, 12], carbides [13, 14], nitrides [15], and silicides [16–19]. Although the configurational entropy is increased through the mixing of metal components in equiatomic ratio, the phase stability of HECs may be dictated by chemical potential, which is the partial derivative of the Gibbs free energy with respect to a particular component, not the configurational entropy or the number of metal components. Tang *et al*, recently investigated the thermodynamic stability of high-entropy carbides via the CALculation of PHAse Diagrams approach and suggested that their formation is controlled by the competition between entropy and enthalpy of mixing [20]. Furthermore, their thermodynamic calculations indicate that many experimentally synthesized high-entropy carbides are not at equilibrium at room temperature.

Recently, the concept of HECs has been expanded to the compositionally-complex ceramics that also include non-equimolar compositions and medium-entropy ceramics [21, 22]. Thus, the terminology of 'HECs' may be better referred to as 'multi-principal component ceramics' to avoid confusions. The main benefits of 'high entropy' ceramics may be the tailorability of physical and chemical properties within a single-phase solid solution.

The compositional complexity in HECs induces significant lattice distortion because of the difference in atomic sizes and bond strengths of the atoms in the M positions. It is worth noting that the chemical bonding in HECs can be a mixture of ionic, covalent, and metallic bonding [11, 23]. In 2015, Rost *et al,* first discovered an entropy stabilized single-phase rock salt structure oxide, $(Mg_{0.2}Co_{0.2}Ni_{0.2}Cu_{0.2}Zn_{0.2})O$, made by quenching [24]. Gild *et al,* first synthesized a family of high-entropy diborides using spark plasma sintering (SPS) in 2016, including $(Hf_{0.2}Zr_{0.2}Ta_{0.2}Mo_{0.2}Ti_{0.2})B_2$ and $(Hf_{0.2}Zr_{0.2}Ta_{0.2}Nb_{0.2}Ti_{0.2})B_2$, which exhibit a single-phase solid solution with a layered hexagonal lattice [11]. In 2018 the high-entropy carbides, including $(Hf_{0.25}Ta_{0.25}Zr_{0.25}Ti_{0.25})C$ and $(Hf_{0.2}Zr_{0.2}Ta_{0.2}Nb_{0.2}Ti_{0.2})C$, were first reported by Yan *et al* [13] and Castle *et al* [25], using SPS from monocarbide powders in equimolar concentrations.

Several excellent reviews already cover high-entropy oxides [26, 27]. For the specific applications in extreme environments, this manuscript focuses on high-entropy carbides and borides. MC-type high-entropy carbides, e.g. $(Hf_{0.2}Zr_{0.2}Ta_{0.2}Nb_{0.2}Ti_{0.2})C$, exhibit a rock-salt B1 structure (figure 1(a), space group $Fm\bar{3}m$), which shares the same cubic structure of most transition metal monocarbides except for δ-WC that has the B_h structure ($P\bar{6}m2$, hexagonal lattice) [28]. The B1 crystal structure of high-entropy carbides has been confirmed by many x-ray diffraction experiments. A neutron diffraction experiment of $(Hf_{0.2}Zr_{0.2}Ta_{0.2}Nb_{0.2}Ti_{0.2})C$ was performed at the Spallation Neutron Source of Oak Ridge National Laboratory using the VULCAN diffractometer [29]. The neutron diffraction result agrees with the rock-salt average structure model, with the C atoms at the (0,0,0) crystallographic site and the metal elements mixed at the (1/2,1/2,1/2) site and fully disordered over the long-range scale. The recent research on high-entropy carbides has revealed reduced thermal conductivity [13], improved hardness [30–32], and an improved oxidation resistance [33–35] compared to transition metal monocarbides, such as ZrC and TiC [36]. These features make them promising candidate materials for extreme environments, such as carbide fuels or fuel claddings in nuclear reactors or thermal protection systems (TPSs) of hypersonic re-entry vehicles.

MB_2-type high-entropy diborides, e.g. $(Hf_{0.2}Zr_{0.2}Ta_{0.2}Mo_{0.2}Ti_{0.2})B_2$, exhibit a hexagonal lattice (figure 1(b), space group P6/mmm). Most of transition metal diborides have the AlB_2-type structure (P6/mmm) while WB_2 forms ReB_2-type ($P6_3/mmc$) structure [37]. The layered AlB_2 structure of high-entropy diborides consists of alternating boron and metallic layers, with mixed covalent and ionic M-B bonds between metal atoms and boron [11]. High-entropy diborides showed better oxidation resistance and higher hardness than the average properties of the individual transitional metal diborides [11]. The potential applications of these high-entropy diborides include scramjet engine components, leading edges [37], TPS for hypersonic vehicles, and solar power concentrators [38].

Despite the extensive research in the recent decade, HECs continue to attract the significant interest of the international scientific community as they can bring new opportunities to enlarge the compositional space of ceramic materials with tailored properties within a single-phase solid solution. The promising properties of HECs have been attributed to the atomic-level disorder, lattice distortion, compositional complexity, and other fundamental processes related to the defect formation and phonon scattering that are still under investigation. The key question is how such an increased number of principal metal elements chemical disorder may influence the physical and chemical properties of HECs. Some characteristics of HECs are similar to HEAs (e.g. lattice distortion), but ceramics may have mixed chemical bonding and unique non-stoichiometry that are more complicated than HEAs. For example, the influence of ionic/covalent bonds and carbon/boron non-stoichiometry on the physical and chemical properties of HECs remain less explored.

This manuscript serves as a critical review of the most recent progress in high-entropy carbides and diborides and

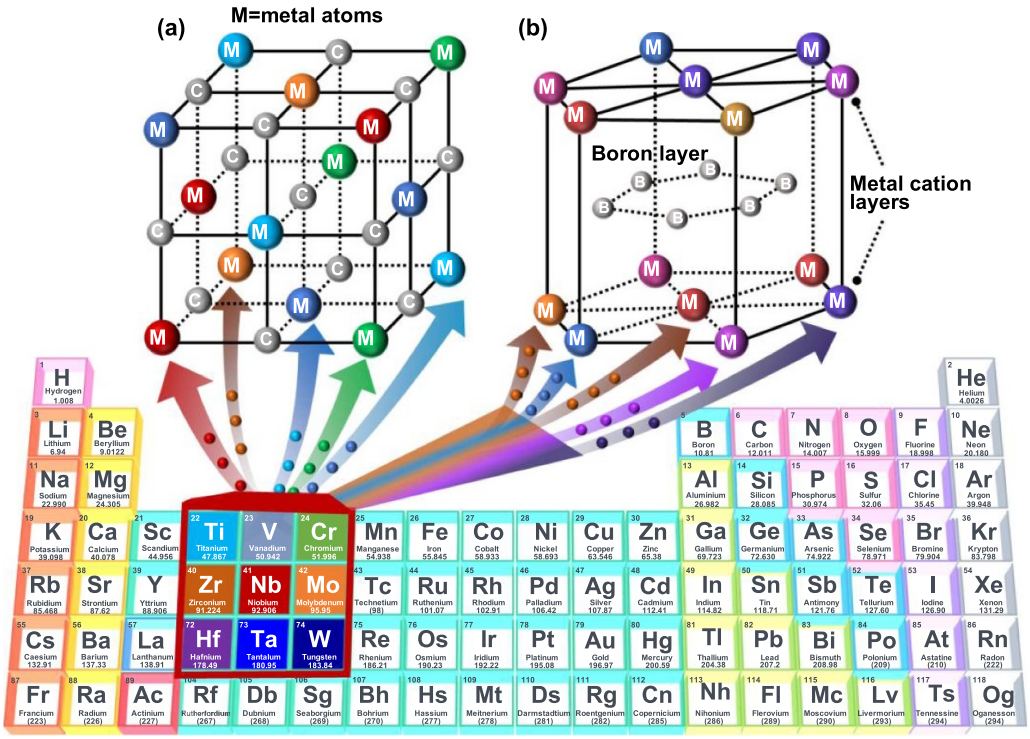

Figure 1. The crystal structure of (a) MC-type high-entropy carbide and (b) MB_2-type high-entropy diboride.

focuses on the evaluation of their performance in extreme environments. It shows that these novel ceramic materials need to be manufactured using high-temperature sintering processes, and some compositions exhibit superior hardness and strength at high temperature and resistance to irradiation damage and oxidizing environments.

2. Synthesis of high-entropy carbides and diborides

Three main synthesis routes of high-entropy carbides have been developed based on the starting raw materials (figure 2): (1) commercial metal carbide powders [13, 23, 25, 29, 32, 39–41]; (2) metallic element and carbon powders [42, 43]; and (3) metal oxide powders and carbon powders. Similarly, the synthesis methods of high-entropy diborides follow three principal routes based on the raw starting materials: (1) commercial metal diboride powders [11]; (2) metallic element and boron powders [44–46]; and (3) metal oxide, carbon, and B_4C powders [44, 46–50]. Wei *et al* [51] compared the high-entropy carbides synthesized from these three routes and found that the microstructures and elements distribution are influenced by the starting materials. Fine starting raw powders result in more homogeneous microstructures and element distribution while introducing a higher oxygen contamination [52]. In all the three synthesis routes, a significant challenge is the residual oxygen content in the as-sintered materials. The final oxygen contamination, which depends on the starting raw powders, is difficult to be fully eliminated during powder processing and high-temperature sintering processes.

After the powder mixtures are processed by ball milling, sintering of high-entropy carbide or diboride powders has been successfully achieved by pressure-assisted techniques including SPS [13, 23, 25, 29, 32, 39–41], hot pressing (HP) [53, 54], and selective laser sintering (SLS) [55]. Both SPS and HP require the aid of temperatures from 1800 °C to 2300 °C to overcome the low diffusion coefficients due to the strong metal–carbon or metal–boron bonding while employing a pressure of tens to hundreds of MPa to better assist final densification. Compared to HP, SPS is able to rapidly producing fully dense materials at a lower temperature in a shorter time [56]. During SPS, a pulsed direct electric current passes through an electrically conductive piston-die assembly (typically made of graphite) and carbide or diboride ceramic powders, which are heated by Joule heating from the electric current passing through them in vacuum environment. Zhang *et al* first developed the SLS process for ultrafast (in seconds) reactive sintering of a single-phase non-equiatomic Zr–Nb–Hf–Ta–C using a Yb fiber laser from a powder mixture of constitute monocarbides [55].

Removing porosity, refining grain size, and getting rid of any contamination are desirable features to obtain superior mechanical and thermal properties of high-entropy carbides and borides. To achieve these results, two important aspects including the purity and particle size of starting powders must be controlled. Smaller particle size will enable a relatively lower sintering temperature and thus less grain growth

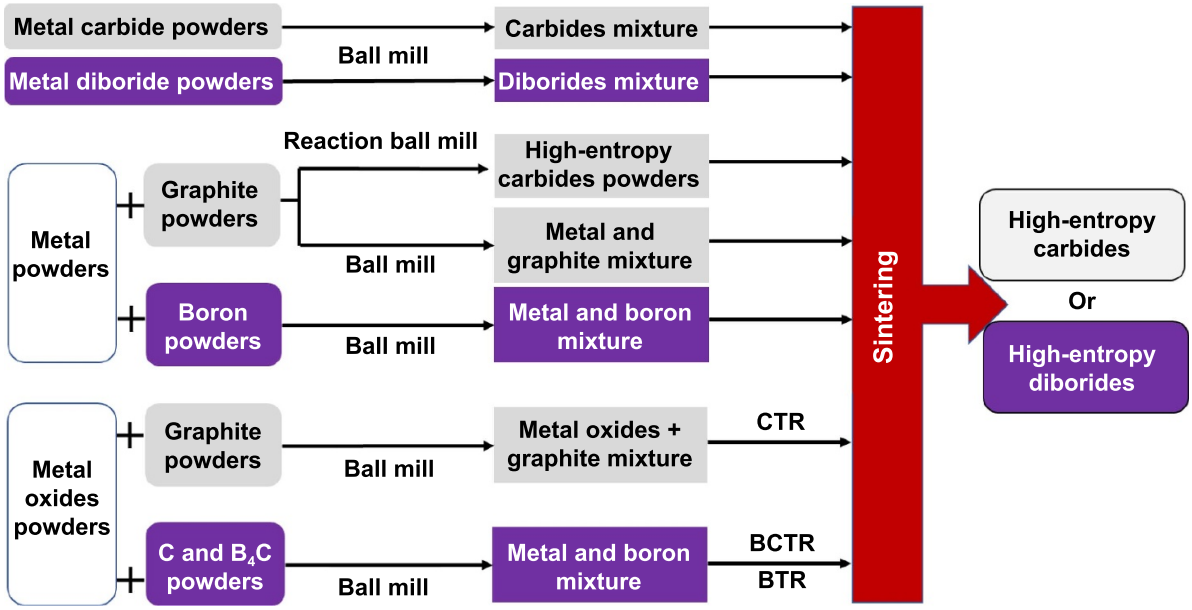

Figure 2. Synthesis routes of high-entropy carbides: carbothermal reduction (CTR), borothermal reaction (BTR) and boro-carbothermal reduction (BCTR).

during sintering [57]. Impurity control, especially oxygen, is crucial during the carbide/boride powder processing and sintering process. Wang *et al* used a two-step SPS technique to sinter $(Hf_{0.2}Zr_{0.2}Ta_{0.2}Nb_{0.2}Ti_{0.2})C$ with a submicron grain size range of 0.4–0.6 μm [29]. Its grain growth kinetics appeared to be limited at 1300 °C and 1600 °C, indicating that the compositional complexity may increase grain boundary complexity and reduce the grain boundary energy. Ma *et al* [58, 59] used high-pressure sintering to synthesize nanocrystalline $(Hf_{0.25}Zr_{0.25}Ta_{0.25}Ti_{0.25})C$ and $(Hf_{0.2}Zr_{0.2}Ta_{0.2}Nb_{0.2}Ti_{0.2})B_2$ ceramics under an external pressure of several GPa, which showed an enhanced hardness because of the grain refinement strengthening [59].

3. Thermal stability

The melting or decomposition temperature of high-entropy carbides and diborides has not been experimentally measured. Liu *et al,* estimated the melting point of quaternary metal carbides from first-principles calculations and predicted that 15 high-entropy carbides have melting point above 3000 °C, in which $(Hf_{0.25}V_{0.25}Nb_{0.25}Ta_{0.25})C$ has the highest melting point of 4400 °C [60]. In a preliminary study, $(Hf_{0.2}Zr_{0.2}Ta_{0.2}Nb_{0.2}Ti_{0.2})C$ samples were annealed at temperatures of 500 °C, 800 °C, 1140 °C, and 1700 °C for two hours under Ar atmosphere. X-ray diffraction analyses indicated no phase transformation at these temperatures, suggesting that this HEC phase is thermally stable from 25 °C to 1700 °C (figure 3). However, the high-entropy materials may have a high activation energy for diffusion and thus long-lasting annealing experiments will be required to study their phase transformation or decomposition behavior at high temperatures.

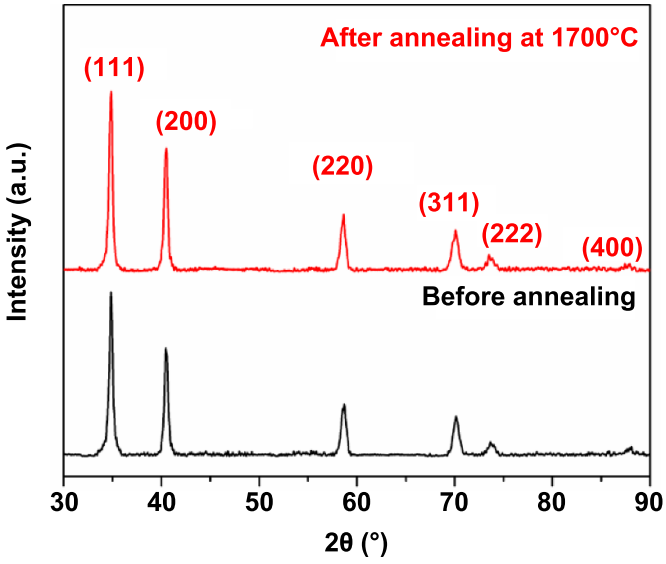

Figure 3. X-ray diffraction patterns of $(Hf_{0.2}Zr_{0.2}Ta_{0.2}Nb_{0.2}Ti_{0.2})C$ before and after annealing at 1700 °C for 2 h in Ar.

4. Mechanical properties

The retention of mechanical properties at elevated temperatures is important because it affects the high-temperature applicability of HECs. The mechanical properties of these ceramics are dependent on the temperature, but also are influenced by microstructure-related factors such as the residual porosity, grain size, and impurities such as undesired oxides. The measured values of hardness, strength and fracture toughness may also depend on the methods selected to test samples. Specifically, the flexural strength is reported to be measured in a 3-point or 4-point bending configuration. However, the

fracture toughness can be measured by single-edge V notched beam (SENVB), chevron notch beam (CNB), and indentation-induced crack measurement (ICM): they give rise to a range of test results where SENVB and CNB are considered more reliable than ICM [61].

At room temperature, the reported data for the fracture toughness and flexural strength of the high-entropy carbides range from 300 to 450 MPa and 3–6 $MPam^{1/2}$, respectively [62, 63]. Higher flexural strength can be achieved through porosity removal and refining the final grain size. When the mean grain size of $(Hf_{0.2}Zr_{0.2}Ta_{0.2}Nb_{0.2}Ti_{0.2})C$ reduced from 16.5 to 0.6 μm, the fracture toughness and flexural strength are increased by 20% and 25%, respectively [29]. The primary fracture mode changed from the trans-granular cleavage to intergranular cracking. High-entropy diborides have reported mean values of 4-point flexural strength of 339–528 MPa, and fracture toughness of 3.6–4.7 MPa $m^{1/2}$ at room temperature [64–67].

The most reported mechanical property of high-entropy carbides and diborides at room temperature is hardness, measured using a Vickers micro-indenter or a Berkovich nano-indenter. The high hardness and elastic modulus of the transition metal carbides, such as HfC, are originated from their strong metal-carbon covalent bonds. The local bonding lengths of each metal–carbon pair in high-entropy carbides may vary around each metal element, causing the chemical bonding effect [68]. It is observed by many studies that the hardness of high-entropy carbides is much higher than the estimated value by the rule-of-mixture [25]. A similar trend is also observed in high-entropy diborides [11]. The enhanced hardness in high-entropy carbides has attracted signification interest. Several mechanisms have been proposed, including mass inhomogeneity [32], solid solution hardening [25], dislocation core atomic randomness [69], and valence electron concentration (VEC) [70]. The mass inhomogeneity in high-entropy carbides may cause impedance mismatch along the path of dislocations, generating reflections and scattering of the activation energy, which results in the increased resistance to plastic deformation macroscopically [32]. The atomic size mismatch in the solid solution [25] causes the lattice distortion, and may limit the motion of dislocations necessary for slip and plastic deformation. Wang *et al* [69] showed that the random interactions between different elements at a dislocation core can increase the barrier to dislocation slip, based on the calculation of Peierls stress of the edge dislocation by density functional theory (DFT). Hossain *et al* [70] suggested that VEC regulates the Fermi energy and alters the bonding characteristics, which was used to design and predict properties of high entropy carbides. The highest hardness is achieved at VEC 8.4.

Flexural strength data of some high-entropy carbides at elevated temperatures have been reported in some studies, suggesting that these ceramics can retain their initial strength up to 1800 °C. Compared to individual monocarbides, some high-entropy carbides show flexural strength retention to higher temperatures (figure 4). However, more test data is needed to compare the flexural strength of high-entropy carbides with that of monocarbides and binary carbides to understand the effects of chemical bonding and compositions. Feng *et al* [71] reported the flexural strength of $(Hf_{0.2}Zr_{0.2}Ta_{0.2}Nb_{0.2}Ti_{0.2})C$ ceramics with relative density of above 99% at elevated temperatures up to 2300 °C. Mean flexural strength was 421 MPa at 25 °C and relatively stable until 1800 °C, before decreasing linearly from 423 MPa at 1800 °C to 318 MPa at 2000 °C and 93 MPa at 2300 °C. Demirskyi *et al* [30, 72] also reported that the average flexural strength of $(Ta_{1/3}Zr_{1/3}Nb_{1/3})C$ with a relative density of 97% was 460 MPa at room temperature, 489 MPa at 1600 °C, then dropped to 366 MPa at 1800 °C and 139 MPa at 2000 °C. The mechanism underlying the strength drop above 1800 °C needs more investigations, which is very likely related to creep deformation or elastic modulus reduction.

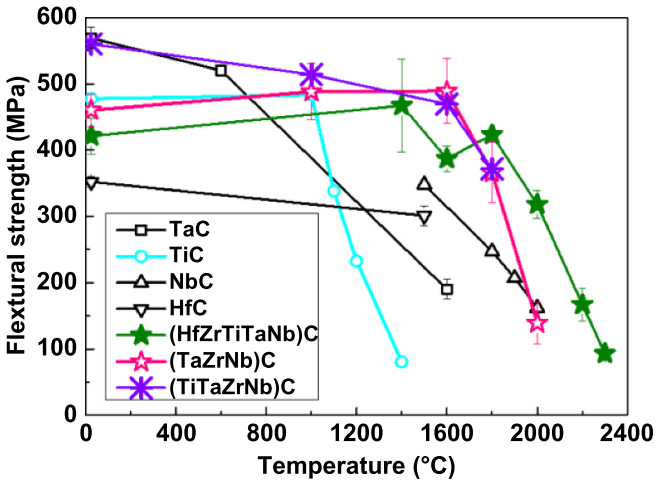

Figure 4. Effect of temperature on the flexural strength of high-entropy carbide vs. monocarbides. The data are summarized from the literature [30, 72–76].

5. Thermal properties

Electrons and phonons are the primary carriers for transferring heat in transition metal carbides. [77] Yan *et al,* first reported in 2018 that the high-entropy carbide, $(Hf_{0.2}Zr_{0.2}Ta_{0.2}Nb_{0.2}Ti_{0.2})C$, showed a significantly reduced thermal diffusivity compared to the monocarbides TaC, ZrC, NbC, TiC, and HfC at room temperature, which was measured by the laser flash technique [13]. Wang *et al,* compared the thermal conductivity of the 4- and 5-metal high-entropy carbides, with the corresponding mono, binary, and ternary carbides as a function of the number of metal elements in carbides from the data in the literature [78], and concluded that the thermal conductivity of transition metal carbides

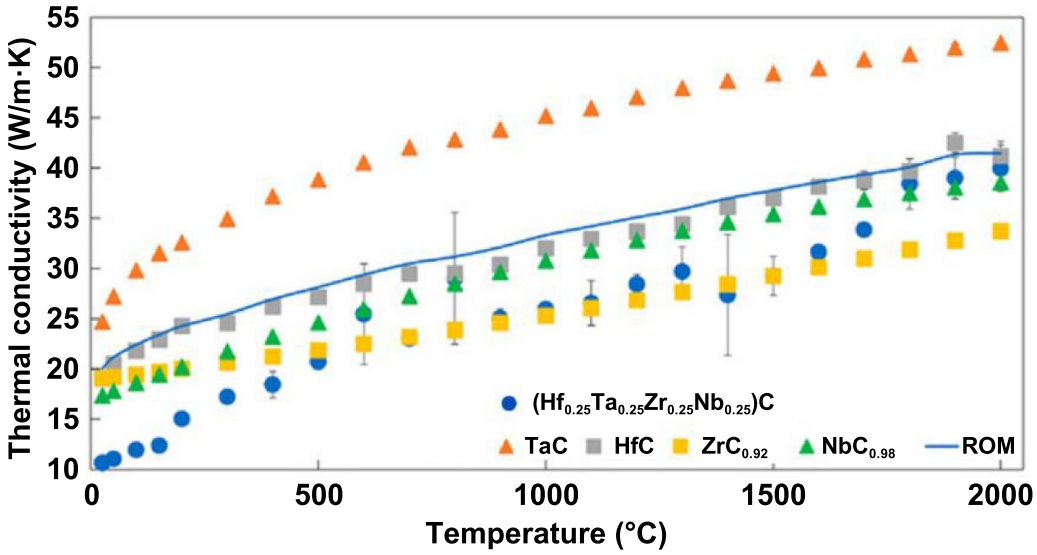

Figure 5. Thermal conductivity of $(Hf_{0.25}Ta_{0.25}Zr_{0.25}Nb_{0.25})C$ from 25 °C to 2000 °C compared to the values of NbC, ZrC, HfC, and TaC along with an average value predicted by a linear molar rule of mixtures (ROM). [82] John Wiley & Sons. © 2022 The American Ceramic Society.

decreases with more metal elements at room temperature. Because of the difference in atomic size and bonding strength of the metal atoms, there exists significant lattice distortions at atomic scale in HECs where atoms of differing characteristics coexist in the same lattice [79]. The fluctuations of mass and interatomic force constants in HECs, due to lattice distortion and the difference in bond strengths, may lead to severe scattering of phonons. It is important to note that the thermal conductivity of transition metal carbide ceramics is also influenced by other defects, such as the porosity, carbon stoichiometry [80], and irradiation-induced defects [81]. Thus, it may be possible to tailor the thermal conductivity of high-entropy carbides by controlling compositions and defects.

The thermal conductivity of $(Hf_{0.25}Ta_{0.25}Zr_{0.25}Nb_{0.25})C$ was measured from 25 °C to 2000 °C, which was lower than the constitute monocarbides except for ZrC that has similar values at 500 to 1600 °C (figure 5) [82, 83]. The contributions of electron and phonon to the thermal conductivity were studied at 25 °C–1600 °C, suggesting that the increase in thermal conductivity with temperature was mainly due to the contribution of electron, while the contribution of phonon exhibited a weak dependence with temperature.

The thermal conductivity of high-entropy diborides was also lower than the constitute diborides. Gild *et al,* showed that the thermal conductivity of single-phase high-entropy diborides at room temperature, $(Hf_{0.2}Zr_{0.2}Ti_{0.2}Ta_{0.2}Cr_{0.2})B_2$, $(Hf_{0.2}Zr_{0.2}Ti_{0.2}Ta_{0.2}Mo_{0.2})B_2$, and $(Hf_{0.2}Zr_{0.2}Ti_{0.2}Ta_{0.2}Nb_{0.2})B_2$, was 12–25 W (m K)$^{-1}$ and only 10% to 20% of the reported data of ZrB_2 and HfB_2 [50]. Zhao *et al,* reported that the thermal conductivity of $(Mo_{0.2}Ta_{0.2}Ni_{0.2}Cr_{0.2}W_{0.2})B$ was 2.05 W (m K)$^{-1}$ at 400 °C, which is much lower than that of the individual borides [84]. Phonon thermal conductivity of $(Ti_{0.2}Zr_{0.2}Hf_{0.2}Nb_{0.2}Ta_{0.2})B_2$ from room temperature to 2400 °C was calculated by the Green–Kubo method [85]. The phonon thermal conductivity along *c* direction is lower than that along *a* direction, which is because the stronger bonding in the basal plane than normal to it. Phonon thermal conductivity of this high-entropy diboride decreases slowly with the temperature.

The thermal expansion coefficient data of HECs is limited and may need more studies to understand the composition effect. The thermal expansion coefficient of $(Hf_{0.2}Zr_{0.2}Ta_{0.2}Nb_{0.2}Ti_{0.2})C$ measured using a dilatometer (6.44×10^{-6} K^{-1}) at room temperature was comparable to that of the five monocarbides (ZrC, HfC, NbC, TiC, and TaC) [13]. Zhang *et al* [77] investigated the temperature-dependent properties of $(Hf_{0.2}Zr_{0.2}Ta_{0.2}Ti_{0.2}M_{0.2})C$, M = Cr, V, Nb, W, or Mo, by DFT calculations: it was shown that $(Hf_{0.2}Zr_{0.2}Ta_{0.2}Ti_{0.2}V_{0.2})C$ has the smallest linear thermal expansion coefficient at high temperature. A temperature-dependent synchrotron-radiation x-ray diffraction analysis was conducted at 298–1273 K to investigate the thermal expansion of a nearly equimolar single-phase $(TiTaNbHfZr)B_2$ [86]. Significant anisotropy between prismatic and basal planes was determined quantitatively. The thermal expansion coefficient of the *a* and *c* directions at 1000 K is 6.5×10^{-6} K^{-1} and 8×10^{-6} K^{-1}, respectively. The behavior of $(TiTaNbHfZr)B_2$ is differently from that expected by the rules for ideal solid solution mixture. Microcracks were found inside the sintered ceramics and interpreted as arising from anisotropic thermal expansion, resulting in thermal residual stresses in the grain matrix that exceeds their failure thresholds. Very recently, Monteverde *et al,* analyzed the anisotropic thermal expansion of a wide spectrum of high-entropy multicomponent AlB_2-type diboride solid solutions [79]: in-plane and out-of-plane non-linear thermal expansion were found to be strongly dependent not only on the chemical complexity and composition but also on the processing conditions.

6. Irradiation resistance

Transition metal carbides such as ZrC are promising candidate materials for the carbide-based composite-type fuels in the gas-cooled fast reactor [87], the coating material for tristructural-isotropic particle fuels in a high-temperature, gas-cooled reactor [88], and (U,Zr)C carbide fuels for space nuclear propulsion [89]. These nuclear applications of carbides result from their high thermal conductivity, high melting temperature, high hydrogen stability, good fission product retention, and outstanding resistance to amorphization [90]. The thermal conductivity of high-entropy carbide becomes close to ZrC at 500 °C–1600 °C (figure 5), which may be suitable for fuel matrix and cladding applications.

Compared to monocarbides, the increasing number of principal metal elements in high-entropy carbides creates atomic-level disorder and a heterogeneous potential energy landscape, which alter vacancy and interstitial migration energies. Consequently, the migration and clustering processes of radiation-induced defects may be suppressed, resulting in slow growth of defect clusters. In HEAs, extensive research has demonstrated that modifying alloy chemical complexity can control the defect production and early-stage damage formation dynamics, finally enhance late-stage radiation tolerance of HEAs under extreme radiation conditions. In particular, the chemical complexity can affect the irradiation defect evolution in five aspects, including the electronic effects (e.g. 3d electronic structures) [83, 91], atomic effects (e.g. atomic-level inhomogeneity and energy landscape [92, 93]), coupled electronic and atomic effects (e.g. nonadiabatic interactions of electrons with ions) [94], defect evolution (e.g. pinning the point defects) [95], and microstructural evolution (e.g. suppressing void swelling and helium bubble growth) [96, 97]. Considering the similarity between HEAs and HECs as well as their significant differences in chemical bonding, some of the similar effects may occur in HECs and are under continuing experimental verifications.

The first studies addressing the irradiation resistance of HECs were conducted in 2019 [40, 98]. Despite substantial variation of the He concentration along the depth of specimen, the diameter of helium bubbles in $(Hf_{0.2}Zr_{0.2}Ta_{0.2}Nb_{0.2}Ti_{0.2})C$ did not exceed 1 nm after irradiation by 120 keV helium ion at room temperature [40]. The motion and coalescence of helium bubbles appeared to be suppressed by the chemical disorder. $(Zr_{0.25}Ta_{0.25}Nb_{0.25}Ti_{0.25})C$ showed high phase stability with no amorphization, phase transformation, or radiation-induced segregation of elements after irradiation by 3 MeV Zr at 25 °C, 300 °C, and 500 °C to 8.0×10^{15} ions cm^{-2} [equal to 20 peak displacements per atom (dpa)] [98]. A relative lattice parameter expansion of ~0.2% was measured by x-ray diffraction. The irradiation-induced microstructure changes were comprised of faulted Frank loops with Burgers vectors $b = a/3\langle 111\rangle$ and perfect dislocation loops with Burgers vectors $b = a/2\langle 110\rangle$ (figure 6) [98]. The dislocation loops remain as small as less than 3 nm under these irradiation conditions, indicating the suppressed clustering and growth of irradiation radiation-induced defects in high-entropy carbides. Very recently Zhu *et al* [99] reported the irradiation damage in $(W_{0.2}Ti_{0.2}V_{0.2}Nb_{0.2}Ta_{0.2})C$ by 1.0 MeV C ions at 25 °C and 650 °C. Relative lattice expansion was introduced by the irradiation and saturated at 0.6%. Irradiation-induced defects were dislocation loops at low dose (<5 dpa) and dislocation networks at higher dose.

It is important to understand the contribution of these irradiation defects to physical properties of high-entropy carbides. However, very few test data has been reported in the literature. Wang *et al,* conducted nanoindentation tests of 3 MeV Zr^{2+}-irradiated $(Zr_{0.25}Ta_{0.25}Nb_{0.25}Ti_{0.25})C$, which showed that the hardness increased by 8%–10% compared to the unirradiated sample [98]. Such an irradiation hardening effect was possibly caused by dislocation loops that hinder the slip movements during the nanoindentations. Dennett *et al* [81] studied the thermal conductivity of 3 MeV Zr^{2+}-irradiated $(Zr_{0.25}Ta_{0.25}Nb_{0.25}Ti_{0.25})C$ using a laser thermal reflectance technique. The reduction in thermal conductivity was observed to be greatest at low irradiation temperatures, suggesting that dislocation loops contribute little to phonon scattering while nanoscale defects serve as more effective scatterers. Overall, the combination of high irradiation resistance with other physical properties such as high strength and hardness may indicate that high-entropy carbides are promising materials for advanced nuclear energy systems.

7. High-temperature oxidation

Since most engine and hypersonic frontier materials are exposed to oxidizing fuels or aviation heating, the non-oxide materials inevitably oxidize and form some combination of solid, liquid, or gaseous reaction products [100, 101]. In real structural applications, very intense temperatures are generated rapidly by burning fuels or viscous flow due to friction with the atmosphere. Therefore, the oxidation resistance is one of the main characteristics associated with the selection of materials for ultra-high temperature ceramics (UHTCs). Oxidation may passivate the underlying substrates by forming protective oxide layers. Dealing with an active mechanism, the reactions do not slow down until the substrate continuously exposed to reactive species is completely consumed [102]. Traditionally, the design of oxidation-resistant materials relies on the existence of elements that can oxidize and form a dense, adherent and protective oxide layers, such as the oxides of Si, Al, and Cr [103].

Current research about the oxidation rate of high-entropy carbides involves oxidation of powder or bulk materials in air [34, 104, 105], oxidation in water vapor [35], and in 1% O_2 partial pressure [104, 106]. Most of the experimental results showed that high-entropy carbides follow the parabolic rate law at 800 °C–1600 °C [33–35, 105, 107], which is related to the diffusion-controlled mass transport mechanisms during the oxidation process. In high-entropy diborides such as $(Zr_{0.2}Hf_{0.2}Ta_{0.2}Nb_{0.2}Ti_{0.2})B_2$ [108] and

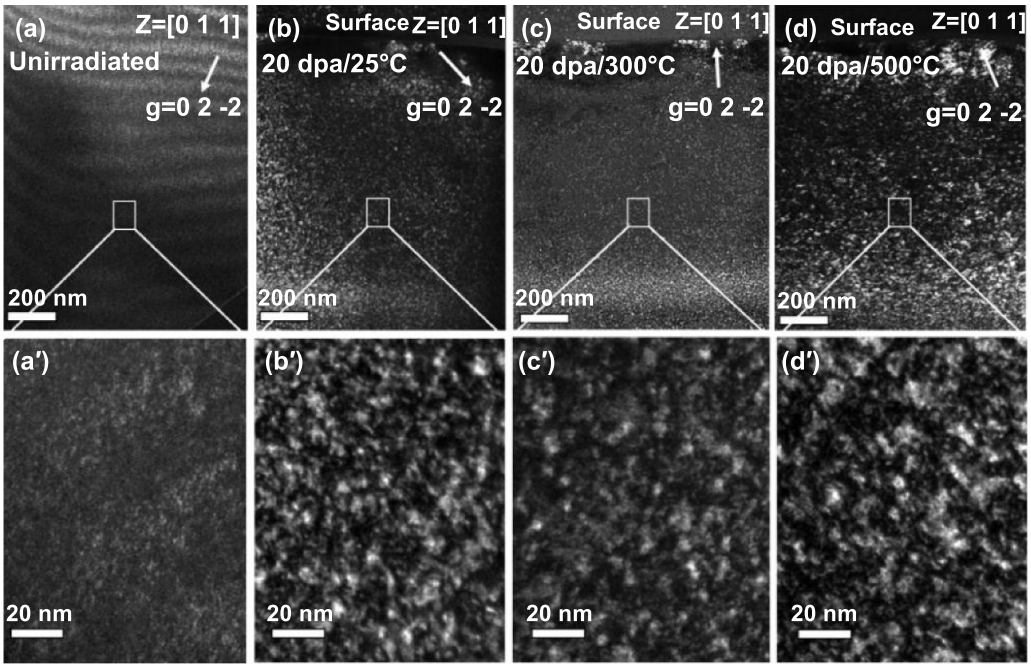

Figure 6. Weak-beam dark-field TEM images of the irradiation-induced dislocation loops in $(Zr_{0.25}Ta_{0.25}Nb_{0.25}Ti_{0.25})C$. Reprinted from [98], Copyright (2020), with permission from Elsevier.

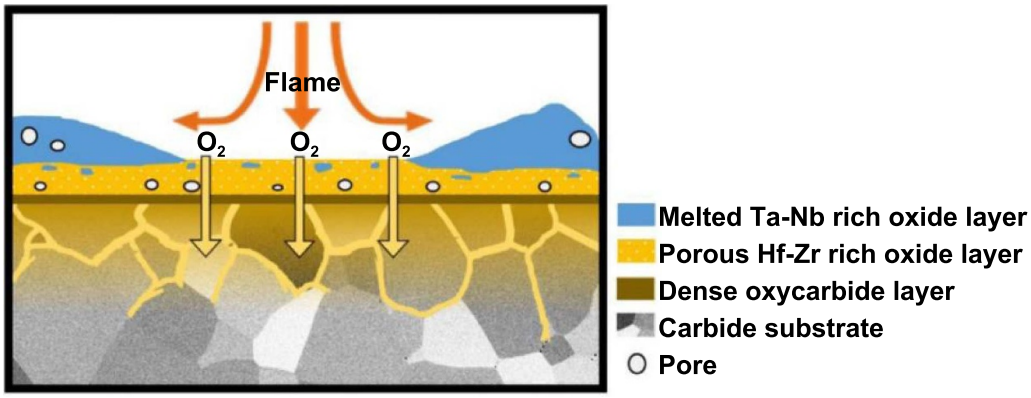

Figure 7. Schematic diagram of ablation mechanism model for $(Hf_{0.25}Ta_{0.25}Zr_{0.25}Nb_{0.25})C$ at 2227 °C. Reprinted from [109], Copyright (2022), with permission from Elsevier.

$(Hf_{0.2}Mo_{0.2}Zr_{0.2}Nb_{0.2}Ti_{0.2})B_2$ [46], there is significant oxidation above 1300 °C due to the volatilization of B_2O_3 in the intermediate temperature range of 1300 °C–1600 °C.

The preferential oxidation behavior in $(Hf_{0.2}Zr_{0.2}Ta_{0.2}Nb_{0.2}Ti_{0.2})C$ and $(Hf_{0.2}Zr_{0.2}Ti_{0.2}Ta_{0.2}Nb_{0.2})B_2$ was studied by Backman *et al* [106] both theoretically and experimentally for 5 min in 1% O_2 atmosphere at 1700 °C. The preferential oxidation of each metal component was related to the relative thermodynamic stability of their corresponding oxides. The group IV metal elements (Hf, Zr, Ti) showed the most favorable formation of oxides because their oxides have the highest melting temperatures and are most thermodynamically favored among the refractory elements. Preferential oxidation also occurred according to relative thermodynamic stability within the group IV metal elements, such as that oxidation of Hf and Zr was more favorable than Ti in high entropy diborides [106]. The preferential oxidation behavior indicates that the high-entropy UHTCs can be designed to form an oxide scale consisting of group IV metal elements.

Oxidation of high-entropy carbides at higher temperature has been investigated by ablation tests at 2000 °C and above. The ablation behavior of $(Hf_{0.25}Ta_{0.25}Zr_{0.25}Nb_{0.25})C$ at 2100 °C [109] showed that Nb–Ta rich oxides were melted and pushed to the edge of the specimen, while Zr–Hf rich oxides with high melting temperature stay in the center of sample to protect the substrate (see figure 7). The ablation resistance of high-entropy carbides can be improved by doping with nitrogen to form carbonitrides: the mass ablation rate of $(Ta_{0.2}Hf_{0.2}Zr_{0.2}Ti_{0.2}Nb_{0.2})C_{0.8}N_{0.2}$ is reduced by 57% than $(Ta_{0.2}Hf_{0.2}Zr_{0.2}Ti_{0.2}Nb_{0.2})C$ at 2227 °C [100]. The enhanced ablation resistance was associated to the formation of a densely packed oxides scale, which contains continuous

Ta, Ti, Nb segregations and large Hf and Zr-rich grains that slow down the inward diffusion of oxygen.

8. Conclusions and outlook

Operations in extreme environments such as in advanced turbine engines, nuclear reactors or vehicles flying at hypersonic speed require to design, synthesize, and process superior materials that can function and outperform an extended lifetime in a complex combination of heat fluxes, chemical reactivities, neutron irradiation, and corrosive coolants. The concept of multi-principal component has led to exploring the center, yet unexplored region of phase diagrams, and providing new possibilities for discovering and developing ceramic materials with novel compositions and superior properties. With a much broader composition space, it becomes viable to tailor their mechanical, thermal, and chemical properties to match the complex requirements in extreme environments.

The key scientific question of how atomic disorder and compositional complexity may influence the physical and chemical properties of high-entropy carbides and borides currently remains poorly understood. While this emerging area has triggered global interest and extensive research in the most recent decade, some fundamental and engineering issues need to be addressed in a short- and long-term timespan:

1. Both computational and experimental investigation are essential to understand the role of the increasing number of principal metal elements, overlapped chemical bonding, and carbon/boron non-stoichiometry on properties of high-entropy carbides or borides. These may cause additional barriers to defect formation and migration, which may control their irradiation damage and oxidation processes.
2. Theoretical research is needed to reveal how the chemical disorder affects the thermal transport, including the nature of heat carriers and their propagation and scattering behavior in a distorted lattice of HECs.
3. Experimental studies are necessary to investigate their deformation behavior, flexural strength, fracture toughness, and creep performance in high temperature and irradiation conditions.
4. New manufacturing processes need to be developed for scale-up synthesis and sintering of HECs to produce near-net-shape components for industry applications. In particular, new opportunities are in the additive manufacturing processes using binders, lasers, and electron beams.
5. The applications of high-entropy carbides and diborides in extreme environments will need to address engineering issues. Whether a HEC is suitable for the specific extreme environment depends on many aspects of material properties and coupled environmental conditions (such as temperature, heat flux, irradiation dose, chemical composition of gases), which needs to be studied by a combination of experimental tests and computational simulations.

Acknowledgments

The information, data, or work presented herein was funded in part by the Advanced Research Projects Agency-Energy (ARPA-E), U.S. Department of Energy, under Award Number DE-AR0001428. The views and opinions of authors expressed herein do not necessarily state or reflect those of the United States Government or any agency thereof. The research was performed in part in the Nebraska Nanoscale Facility: National Nanotechnology Coordinated Infrastructure and the Nebraska Center for Materials and Nanoscience (and/or NERCF), which are supported by the National Science Foundation under Award ECCS: 2025298, and the Nebraska Research Initiative.

ORCID iDs

Frederic Monteverde https://orcid.org/0000-0002-9766-2275
Bai Cui https://orcid.org/0000-0002-0585-6698

References

[1] Zhang Y W, Zhao S J, Weber W J, Nordlund K, Granberg F and Djurabekova F 2017 Atomic-level heterogeneity and defect dynamics in concentrated solid-solution alloys *Curr. Opin. Solid State Mater. Sci.* **21** 221–37
[2] Zhang Y, Zuo T T, Tang Z, Gao M C, Dahmen K A, Liaw P K and Lu Z P 2014 Microstructures and properties of high-entropy alloys *Prog. Mater. Sci.* **61** 1–93
[3] Tsai M H and Yeh J W 2014 High-entropy alloys: a critical review *Mater. Res. Lett.* **2** 107–23
[4] Kumar N A P K, Li C, Leonard K J, Bei H and Zinkle S J 2016 Microstructural stability and mechanical behavior of FeNiMnCr high entropy alloy under ion irradiation *Acta Mater.* **113** 230–44
[5] Lu Y P *et al* 2019 A promising new class of irradiation tolerant materials: $Ti_2ZrHfV_{0.5}Mo_{0.2}$ high-entropy alloy *J. Mater. Sci. Technol.* **35** 369–73
[6] Jiang B, Wang W, Liu S X, Wang Y, Wang C F, Chen Y N, Xie L, Huang M Y and He J Q 2022 High figure-of-merit and power generation in high-entropy GeTe-based thermoelectrics *Science* **377** 208–13
[7] Zhang L, Shi X L, Yang Y L and Chen Z G 2021 Flexible thermoelectric materials and devices: from materials to applications *Mater. Today* **46** 62–108
[8] Jiang B B *et al* 2021 High-entropy-stabilized chalcogenides with high thermoelectric performance *Science* **371** 830–4
[9] Bérardan D, Franger S, Dragoe D, Meena A K and Dragoe N 2016 Colossal dielectric constant in high entropy oxides *Phys. Status Solidi* **10** 328–33
[10] Bérardan D, Franger S, Meena A K and Dragoe N 2016 Room temperature lithium superionic conductivity in high entropy oxides *J. Mater. Chem.* **4** 9536–41
[11] Gild J, Zhang Y Y, Harrington T, Jiang S C, Hu T, Quinn M C, Mellor W M, Zhou N X, Vecchio K and Luo J 2016 High-entropy metal diborides: a new class of high-entropy materials and a new type of ultrahigh temperature ceramics *Sci. Rep.* **6** 37946
[12] Gild J, Kaufmann K, Vecchio K and Luo J 2019 Reactive flash spark plasma sintering of high-entropy ultrahigh temperature ceramics *Scr. Mater.* **170** 106–10
[13] Yan X L, Constantin L, Lu Y F, Silvain J F, Nastasi M and Cui B 2018 $(Hf_{0.2}Zr_{0.2}Ta_{0.2}Nb_{0.2}Ti_{0.2})C$ high-entropy

ceramics with low thermal conductivity *J. Am. Ceram. Soc.* **101** 4486–91
[14] Zhou J Y, Zhang J Y, Zhang F, Niu B, Lei L W and Wang W M 2018 High-entropy carbide: a novel class of multicomponent ceramics *Ceram. Int.* **44** 22014–8
[15] Jin T, Sang X H, Unocic R R, Kinch R T, Liu X F, Hu J, Liu H L and Dai S 2018 Mechanochemical-assisted synthesis of high-entropy metal nitride via a soft urea strategy *Adv. Mater.* **30** 1707512
[16] Liu L, Zhang L Q and Liu D 2020 Complete elimination of pest oxidation by high entropy refractory metallic silicide $(Mo_{0.2}W_{0.2}Cr_{0.2}Ta_{0.2}Nb_{0.2})Si_2$ *Scr. Mater.* **189** 25–29
[17] Qin Y, Wang J C, Liu J X, Wei X F, Li F, Zhang G J, Jing C X, Zhao J W and Wu H Z 2020 High-entropy silicide ceramics developed from $(TiZrNbMoW)Si_2$ formulation doped with aluminum *J. Eur. Ceram. Soc.* **40** 2752–9
[18] Qin Y, Liu J X, Li F, Wei X F, Wu H and Zhang G J 2019 A high entropy silicide by reactive spark plasma sintering *J. Adv. Ceram.* **8** 148–52
[19] Gild J, Braun J, Kaufmann K, Marin E, Harrington T, Hopkins P, Vecchio K and Luo J 2019 A high-entropy silicide: $(Mo_{0.2}Nb_{0.2}Ta_{0.2}Ti_{0.2}W_{0.2})Si_2$ *J. Mater.* **5** 337–43
[20] Tang X C, Thompson G B, Ma K K and Weinberger C R 2022 The role of entropy and enthalpy in high entropy carbides *Comput. Mater. Sci.* **210** 111474
[21] Wright A J, Wang Q Y, Huang C Y, Nieto A, Chen R K and Luo J 2020 From high-entropy ceramics to compositionally-complex ceramics: a case study of fluorite oxides *J. Eur. Ceram. Soc.* **40** 2120–9
[22] Wright A J and Luo J 2020 A step forward from high-entropy ceramics to compositionally complex ceramics: a new perspective *J. Mater. Sci.* **55** 9812–27
[23] Ye B L, Wen T Q, Huang K H, Wang C Z and Chu Y H 2019 First-principles study, fabrication, and characterization of $(Hf_{0.2}Zr_{0.2}Ta_{0.2}Nb_{0.2}Ti_{0.2})C$ high-entropy ceramic *J. Am. Ceram. Soc.* **102** 4344–52
[24] Rost C M, Sachet E, Borman T, Moballegh A, Dickey E C, Hou D, Jones J L, Curtarolo S and Maria J P 2015 Entropy-stabilized oxides *Nat. Commun.* **6** 8485
[25] Castle E, Csanádi T, Grasso S, Dusza J and Reece M 2018 Processing and properties of high-entropy ultra-high temperature carbides *Sci. Rep.* **8** 8609
[26] Sarkar A, Wang Q S, Schiele A, Chellali M R, Bhattacharya S S, Wang D, Brezesinski T, Hahn H, Velasco L and Breitung B 2019 High-entropy oxides: fundamental aspects and electrochemical properties *Adv. Mater.* **31** 1806236
[27] Albedwawi S H, AlJaberi A, Haidemenopoulos G N and Polychronopoulou K 2021 High entropy oxides-exploring a paradigm of promising catalysts: a review *Mater. Des.* **202** 109534
[28] Kurlov A S and Gusev A I 2006 Tungsten carbides and W-C phase diagram *Inorg. Mater.* **42** 121–7
[29] Wang F, Zhang X, Yan X, Lu Y, Nastasi M, Chen Y and Cui B 2020 The effect of submicron grain size on thermal stability and mechanical properties of high-entropy carbide ceramics *J. Am. Ceram. Soc.* **103** 4463–72
[30] Demirskyi D, Borodianska H, Suzuki T S, Sakka Y, Yoshimi K and Vasylkiv O 2019 High-temperature flexural strength performance of ternary high-entropy carbide consolidated via spark plasma sintering of TaC, ZrC and NbC *Scr. Mater.* **164** 12–16
[31] Yang Y, Wang W, Gan G Y, Shi X F and Tang B Y 2018 Structural, mechanical and electronic properties of (TaNbHfTiZr)C high entropy carbide under pressure: *ab initio* investigation *Physica* B **550** 163–70
[32] Sarker P, Harrington T, Toher C, Oses C, Samiee M, Maria J P, Brenner D W, Vecchio K S and Curtarolo S 2018 High-entropy high-hardness metal carbides discovered by entropy descriptors *Nat. Commun.* **9** 4980
[33] Ye B L, Wen T Q and Chu Y H 2020 High-temperature oxidation behavior of $(Hf_{0.2}Zr_{0.2}Ta_{0.2}Nb_{0.2}Ti_{0.2})C$ high-entropy ceramics in air *J. Am. Ceram. Soc.* **103** 500–7
[34] Ye B L, Wen T Q, Liu D and Chu Y H 2019 Oxidation behavior of $(Hf_{0.2}Zr_{0.2}Ta_{0.2}Nb_{0.2}Ti_{0.2})C$ high-entropy ceramics at 1073-1473 K in air *Corros. Sci.* **153** 327–32
[35] Tan Y Q, Chen C, Li S G, Han X C, Xue J X, Liu T, Zhou X S and Zhang H B 2020 Oxidation behaviours of high-entropy transition metal carbides in 1200 °C water vapor *J. Alloys Compd.* **816** 152523
[36] Xiang H, Xing Y, Dai F, Wang H and Su L 2021 High-entropy ceramics: present status, challenges, and a look forward *J. Adv. Ceram.* **10** 385–441
[37] Pangilinan L E, Turner C L, Akopov G, Anderson M, Mohammadi R and Kaner R B 2018 Superhard tungsten diboride-based solid solutions *Inorg. Chem.* **57** 15305–13
[38] Fahrenholtz W G, Hilmas G E and Li R X 2020 Densification of ultra-refractory transition metal diboride ceramics *Sci. Sinter.* **52** 1–14
[39] Ye B L, Wen T Q, Nguyen M C, Hao L Y, Wang C Z and Chu Y H 2019 First-principles study, fabrication and characterization of $(Zr_{0.25}Nb_{0.25}Ti_{0.25}V_{0.25})C$ high-entropy ceramics *Acta Mater.* **170** 15–23
[40] Wang F, Yan X L, Shao L, Nastasi M and Cui B 2019 Irradiation damage behavior in novel high-entropy carbide ceramics *Trans. Am. Nucl. Soc.* **120** 327
[41] Harrington T J *et al* 2019 Phase stability and mechanical properties of novel high entropy transition metal carbides *Acta Mater.* **166** 271–80
[42] Moskovskikh D O, Vorotilo S, Sedegov A S, Kuskov K V, Bardasova K V, Kiryukhantsev-Korneev P V, Zhukovskyi M and Mukasyan A S 2020 High-entropy (HfTaTiNbZr)C and (HfTaTiNbMo)C carbides fabricated through reactive high-energy ball milling and spark plasma sintering *Ceram. Int.* **46** 19008–14
[43] Liu D Q, Zhang A J, Jia J G, Meng J H and Su B 2020 Phase evolution and properties of (VNbTaMoW)C high entropy carbide prepared by reaction synthesis *J. Eur. Ceram. Soc.* **40** 2746–51
[44] Barbarossa S, Orrù R, Garroni S, Licheri R and Cao G 2021 Ultra high temperature high-entropy borides: effect of graphite addition on oxides removal and densification behaviour *Ceram. Int.* **47** 6220–31
[45] Tallarita G, Licheri R, Garroni S, Orrù R and Cao G 2019 Novel processing route for the fabrication of bulk high-entropy metal diborides *Scr. Mater.* **158** 100–4
[46] Tallarita G, Licheri R, Garroni S, Barbarossa S, Orrù R and Cao G 2020 High-entropy transition metal diborides by reactive and non-reactive spark plasma sintering: a comparative investigation *J. Eur. Ceram. Soc.* **40** 942–52
[47] Zhang Y, Guo W M, Jiang Z B, Zhu Q Q, Sun S K, You Y, Plucknett K and Lin H T 2019 Dense high-entropy boride ceramics with ultra-high hardness *Scr. Mater.* **164** 135–9
[48] Gu J F, Zou J, Sun S K, Wang H, Yu S Y, Zhang J Y, Wang W M and Fu Z Y 2019 Dense and pure high-entropy metal diboride ceramics sintered from self-synthesized powders *via* boro/carbothermal reduction approach *Sci. China Mater.* **62** 1898–909
[49] Feng L, Fahrenholtz W G and Hilmas G E 2020 Processing of dense high-entropy boride ceramics *J. Eur. Ceram. Soc.* **40** 3815–23
[50] Gild J *et al* 2020 Thermal conductivity and hardness of three single-phase high-entropy metal diborides fabricated by borocarbothermal reduction and spark plasma sintering *Ceram. Int.* **46** 6906–13

[51] Wei X F, Liu J X, Li F, Qin Y, Liang Y C and Zhang G J 2019 High entropy carbide ceramics from different starting materials *J. Eur. Ceram. Soc.* **39** 2989–94

[52] Wei X F, Qin Y, Liu J X, Li F, Liang Y C and Zhang G J 2020 Gradient microstructure development and grain growth inhibition in high-entropy carbide ceramics prepared by reactive spark plasma sintering *J. Eur. Ceram. Soc.* **40** 935–41

[53] Monteverde F and Saraga F 2020 Entropy stabilized single-phase (Hf, Nb, Ta, Ti, Zr)B_2 solid solution powders obtained via carbo/boro-thermal reduction *J. Alloys Compd.* **824** 153930

[54] Monteverde F, Saraga F and Gaboardi M 2020 Compositional disorder and sintering of entropy stabilized (Hf, Nb, Ta, Ti, Zr)B_2 solid solution powders *J. Eur. Ceram. Soc.* **40** 3807–14

[55] Zhang X, Li N, Chen X, Stroup M, Lu Y F and Cui B 2023 Direct selective laser sintering of high-entropy carbide ceramics *J. Mater. Res.* **38** 187–97

[56] Munir Z A, Anselmi-Tamburini U and Ohyanagi M 2006 The effect of electric field and pressure on the synthesis and consolidation of materials: a review of the spark plasma sintering method *J. Mater. Sci.* **41** 763–77

[57] Feng L, Lee S H and Kim H N 2017 Effects of high-energy ball milling and reactive spark plasma sintering on the densification of HfC-SiC composites *J. Eur. Ceram. Soc.* **37** 1891–8

[58] Ma M D, Ye B L, Han Y J, Sun L, He J L and Chu Y H 2020 High-pressure sintering of ultrafine-grained high-entropy diboride ceramics *J. Am. Ceram. Soc.* **103** 6655–8

[59] Ma M D, Sun Y N, Wu Y J, Zhao Z S, Ye L and Chu Y H 2022 Nanocrystalline high-entropy carbide ceramics with improved mechanical properties *J. Am. Ceram. Soc.* **105** 606–13

[60] Liu S Y, Zhang S X, Liu S Y, Li D J, Li Y P and Wang S W 2021 Phase stability, mechanical properties and melting points of high-entropy quaternary metal carbides from first-principles *J. Eur. Ceram. Soc.* **41** 6267–74

[61] Quinn G D and Bradt R C 2007 On the Vickers indentation fracture toughness test *J. Am. Ceram. Soc.* **90** 673–80

[62] Nisar A, Zhang C, Boesl B and Agarwal A 2020 A perspective on challenges and opportunities in developing high entropy-ultra high temperature ceramics *Ceram. Int.* **46** 25845–53

[63] Feng L, Fahrenholtz W G and Brenner D W 2021 High-entropy ultra-high-temperature borides and carbides: a new class of materials for extreme environments *Annu. Rev. Mater. Res* **51** 165–85

[64] Zhang Y, Jiang Z B, Sun S K, Guo W M, Chen Q S, Qiu J X, Plucknett K and Lin H T 2019 Microstructure and mechanical properties of high-entropy borides derived from boro/carbothermal reduction *J. Eur. Ceram. Soc.* **39** 3920–4

[65] Qiao L J, Liu Y, Gao Y, Bi J Q, Li Y H, Liu C, Gao J, Wang W L and Qian Z 2022 First-principles prediction, fabrication and characterization of $(Hf_{0.2}Nb_{0.2}Ta_{0.2}Ti_{0.2}Zr_{0.2})B_2$ high-entropy borides *Ceram. Int.* **48** 17234–45

[66] Liu J X, Shen X Q, Wu Y, Li F, Liang Y C and Zhang G J 2020 Mechanical properties of hot-pressed high-entropy diboride-based ceramics *J. Adv. Ceram.* **9** 503–10

[67] Murchie A C, Watts J L, Fahrenholtz W G and Hilmas G E 2022 Room-temperature mechanical properties of a high-entropy diboride *Int. J. Appl. Ceram. Technol.* **19** 2293–9

[68] Rost C M, Rak Z, Brenner D W and Maria J P 2017 Local structure of the $Mg_xNi_xCo_xCu_xZn_xO$ ($x = 0.2$) entropy-stabilized oxide: an EXAFS study *J. Am. Ceram. Soc.* **100** 2732–8

[69] Wang Y C, Csanádi T, Zhang H F, Dusza J, Reece M J and Zhang R Z 2020 Enhanced hardness in high-entropy carbides through atomic randomness *Adv. Theory Simul.* **3** 2000111

[70] Hossain M D, Lowum S, Borman T and Maria J P 2021 Fermi level engineering and mechanical properties of high entropy carbides (arXiv: 2101.04885)

[71] Feng L, Chen W T, Fahrenholtz W G and Hilmas G E 2021 Strength of single-phase high-entropy carbide ceramics up to 2300 °C *J. Am. Ceram. Soc.* **104** 419–27

[72] Demirskyi D, Suzuki T S, Yoshimi K and Vasylkiv O 2020 Synthesis and high-temperature properties of medium-entropy (Ti, Ta, Zr, Nb)C using the spark plasma consolidation of carbide powders *Open Ceram.* **2** 100015

[73] Miracle D B and Lipsitt H A 1983 Mechanical properties of fine-grained substoichiomebic titanium carbide *J. Am. Ceram. Soc.* **66** 592–7

[74] Katz A P, Lipsitt H A, Mah T and Mendiratta M G 1983 Mechanical behaviour of polycrystalline TiC *J. Mater. Sci.* **18** 1983–92

[75] Silvestroni L, Bellosi A, Melandri C, Sciti D, Liu J X and Zhang G J 2011 Microstructure and properties of HfC and TaC-based ceramics obtained by ultrafine powder *J. Eur. Ceram. Soc.* **31** 619–27

[76] Kelly A and Rowcliffe D J 1967 Deformation of poly crystalline transition metal carbides *J. Am. Ceram. Soc.* **50** 253–6

[77] Zhang P X, Ye L, Chen F H, Han W J, Wu Y H and Zhao T 2022 Stability, mechanical, and thermodynamic behaviors of (TiZrHfTaM)C (M = Nb,Mo,W,V,Cr) high-entropy carbide ceramics *J. Alloys Compd.* **903** 163868

[78] Wang Y C 2022 Processing and properties of high entropy carbides *Adv. Appl. Ceram.* **121** 57–78

[79] Monteverde F, Gaboardi M, Saraga F, Feng L, Fahrenholtz W and Hilmas G 2022 Anisotropic thermal expansion in high-entropy multicomponent AlB_2-type diboride solid solutions *Int. J. Extrem. Manuf.* **5** 015505

[80] Rost C M, Borman T, Hossain M D, Lim M, Quiambao-Tomko K F, Tomko J A, Brenner D W, Maria J P and Hopkins P E 2020 Electron and phonon thermal conductivity in high entropy carbides with variable carbon content *Acta Mater.* **196** 231–9

[81] Dennett C A, Hua Z L, Lang E, Wang F and Cui B 2022 Thermal conductivity reduction in $(Zr_{0.25}Ta_{0.25}Nb_{0.25}Ti_{0.25})C$ high entropy carbide from extrinsic lattice defects *Mater. Res. Lett.* **10** 611–7

[82] Schwind E C, Reece M J, Castle E, Fahrenholtz W G and Hilmas G E 2022 Thermal and electrical properties of a high entropy carbide (Ta, Hf, Nb, Zr) at elevated temperatures *J. Am. Ceram. Soc.* **105** 4426–34

[83] Zhou Y, Fahrenholtz W G, Graham J and Hilmas G E 2021 From thermal conductive to thermal insulating: Effect of carbon vacancy content on lattice thermal conductivity of ZrCx *J. Mater. Sci. Technol.* **82** 105–13

[84] Zhao P B *et al* 2020 A novel high-entropy monoboride $(Mo_{0.2}Ta_{0.2}Ni_{0.2}Cr_{0.2}W_{0.2})B$ with superhardness and low thermal conductivity *Ceram. Int.* **46** 26626–31

[85] Dai F Z, Sun Y J, Wen B, Xiang H M and Zhou Y C 2021 Temperature dependent thermal and elastic properties of high entropy $(Ti_{0.2}Zr_{0.2}Hf_{0.2}Nb_{0.2}Ta_{0.2})B_2$: molecular dynamics simulation by deep learning potential *J. Mater. Sci. Technol.* **72** 8–15

[86] Monteverde F, Saraga F, Gaboardi M and Plaisier J R 2021 Compositional pathways and anisotropic thermal expansion of high-entropy transition metal diborides *J. Eur. Ceram. Soc.* **41** 6255–66

[87] Weaver K D *et al* 2004 *Gas-Cooled Fast Reactor (GFR) FY04 Annual Report* (Idaho National Lab: Idaho Falls, ID)

[88] Sawa K and Ueta S 2004 Research and development on HTGR fuel in the HTTR project *Nucl. Eng. Des.* **233** 163–72

[89] Anghaie S and Knight T 2002 Status of advanced carbide fuels: past, present, and future *AIP Conf. Proc.* **608** 852–6

[90] Zheng M J, Szlufarska I and Morgan D 2015 Defect kinetics and resistance to amorphization in zirconium carbide *J. Nucl. Mater.* **457** 343–51

[91] Mu S, Yin J, Samolyuk G D, Wimmer S, Pei Z, Eisenbach M, Mankovsky S, Ebert H and Stocks G M 2019 Hidden Mn magnetic-moment disorder and its influence on the physical properties of medium-entropy NiCoMn solid solution alloys *Phys. Rev. Mater.* **3** 014411

[92] Velişa G, Wendler E, Zhao S, Jin K, Bei H, Weber W J and Zhang Y 2018 Delayed damage accumulation by athermal suppression of defect production in concentrated solid solution alloys *Mater. Res. Lett.* **6** 136–41

[93] Oh H S *et al* 2019 Engineering atomic-level complexity in high-entropy and complex concentrated alloys *Nat. Commun.* **10** 2090

[94] Ullah R, Artacho E and Correa A A 2018 Core electrons in the electronic stopping of heavy ions *Phys. Rev. Lett.* **121** 116401

[95] Yang T N, Lu C Y, Velisa G, Jin K, Xiu P Y, Crespillo M L, Zhang Y W, Bei H B and Wang L M 2018 Effect of alloying elements on defect evolution in Ni-20X binary alloys *Acta Mater.* **151** 159–68

[96] Fan Z, Zhao S J, Jin K, Chen D, Osetskiy Y N, Wang Y Q, Bei H B, More K L and Zhang Y W 2019 Helium irradiated cavity formation and defect energetics in Ni-based binary single-phase concentrated solid solution alloys *Acta Mater.* **164** 283–92

[97] Lu C Y *et al* 2018 Enhanced void swelling in NiCoFeCrPd high-entropy alloy by indentation-induced dislocations *Mater. Res. Lett.* **6** 584–91

[98] Wang F, Yan X L, Wang T Y, Wu Y Q, Shao L, Nastasi M, Lu Y F and Cui B 2020 Irradiation damage in $(Zr_{0.25}Ta_{0.25}Nb_{0.25}Ti_{0.25})C$ high-entropy carbide ceramics *Acta Mater.* **195** 739–49

[99] Zhu Y B, Chai J L, Wang Z G, Shen T L, Niu L J, Li S F, Jin P, Zhang H P, Li J and Cui M H 2022 Microstructural damage evolution of $(WTiVNbTa)C_5$ high-entropy carbide ceramics induced by self-ions irradiation *J. Eur. Ceram. Soc.* **42** 2567–76

[100] Peng Z, Sun W, Xiong X, Zhang H B, Guo F W and Li J M 2021 Novel refractory high-entropy ceramics: transition metal carbonitrides with superior ablation resistance *Corros. Sci.* **184** 109359

[101] Wuchina E, Opila E, Opeka M, Fahrenholtz W and Talmy I 2007 UHTCs: ultra-high temperature ceramic materials for extreme environment applications *Electrochem. Soc. Interface* **16** 30–36

[102] Lee W E and Rainforth W M 1994 *Ceramic Microstructures: Property Control by Processing* (Dordrecht: Springer)

[103] Cui B 2011 *Microstructural Evolution and Oxidation Behaviour of Spark Plasma Sintered Mn+1AXn Ceramics* (London: Imperial College London) (https://doi.org/10.25560/9110)

[104] Wang Y C and Reece M J 2021 Oxidation resistance of (Hf-Ta-Zr-Nb)C high entropy carbide powders compared with the component monocarbides and binary carbide powders *Scr. Mater.* **193** 86–90

[105] Wang Y C, Zhang R Z, Zhang B H, Skurikhina O, Balaz P, Araullo-Peters V and Reece M J 2020 The role of multi-elements and interlayer on the oxidation behaviour of (Hf-Ta-Zr-Nb)C high entropy ceramics *Corros. Sci.* **176** 109019

[106] Backman L, Gild J, Luo J and Opila E J 2020 Part II: experimental verification of computationally predicted preferential oxidation of refractory high entropy ultra-high temperature ceramics *Acta Mater.* **197** 81–90

[107] Wang H X, Cao Y J, Liu W and Wang Y G 2020 Oxidation behavior of $(Hf_{0.2}Ta_{0.2}Zr_{0.2}Ti_{0.2}Nb_{0.2})C$-xSiC ceramics at high temperature *Ceram. Int.* **46** 11160–8

[108] Guo R R, Li Z J, Li L, Liu Y, Zheng R X and Ma C L 2022 Microstructures and oxidation mechanisms of $(Zr_{0.2}Hf_{0.2}Ta_{0.2}Nb_{0.2}Ti_{0.2})B_2$ high-entropy ceramic *J. Eur. Ceram. Soc.* **42** 2127–34

[109] Wang Y C, Zhang B H, Zhang C Y, Yin J and Reece M J 2022 Ablation behaviour of (Hf-Ta-Zr-Nb)C high entropy carbide ceramic at temperatures above 2100 °C *J. Mater. Sci. Technol.* **113** 40–47